Geophysical Research Letters®

RESEARCH LETTER
10.1029/2021GL094969

Key Points:

- The tropical temperature profile in the free troposphere deviates from that following a moist-adiabatic lapse rate (LR)
- The deviations from the moist-adiabatic LR can be explained by entrainment with a buoyancy-sorting mechanism
- The temperature deviations from moist-adiabats increase climate sensitivity

Supporting Information:

Supporting Information may be found in the online version of this article.

Correspondence to:

J. Bao,
jiawei.bao@mpimet.mpg.de

Citation:

Bao, J., Stevens, B., Kluft, L., & Jiménez-de-la-Cuesta, D. (2021). Changes in the tropical lapse rate due to entrainment and their impact on climate sensitivity. *Geophysical Research Letters*, *48*, e2021GL094969. https://doi.org/10.1029/2021GL094969

Received 23 JUN 2021
Accepted 27 AUG 2021

Changes in the Tropical Lapse Rate due to Entrainment and Their Impact on Climate Sensitivity

Jiawei Bao[1], Bjorn Stevens[1], Lukas Kluft[1], and Diego Jiménez-de-la-Cuesta[1]

[1]Max Planck Institute for Meteorology, Hamburg, Germany

Abstract The tropical temperature in the free troposphere deviates from a theoretical moist-adiabat. The overall deviations are attributed to the entrainment of dry surrounding air. The deviations gradually approach zero in the upper troposphere, which we explain with a buoyancy-sorting mechanism: the height to which individual convective parcels rise depends on parcel buoyancy, which is closely tied to the impact of entrainment during ascent. In higher altitudes, the temperature is increasingly controlled by the convective parcels that are warmer and more buoyant because of weaker entrainment effects. We represent such temperature deviations from moist-adiabats in a clear-sky one-dimensional radiative-convective equilibrium model. Compared with a moist-adiabatic adjustment, having the entrainment-induced temperature deviations lead to higher clear-sky climate sensitivity. As the impact of entrainment depends on the saturation deficit, which increases with warming, our model predicts even more amplified surface warming from entrainment in a warmer climate.

Plain Language Summary The tropical temperature structure is determined by regions with deep convection, which is believed to be moist-adiabatic. However, both models and observations show that the temperature deviates from moist-adiabats. This is because convective parcels often mix with dry environmental air during ascent, pushing the temperature away from the moist-adiabatic structure. More importantly, the tropical temperature is not dominated by one or a few strongest convective plumes, but rather controlled by the combined effect of many convective plumes of different strengths and depths. Therefore, the tropical temperature structure reflects the composition of convection happening at different values of boundary-layer energy and mixing processes of variable efficiency with the environment. Using an idealized model, we find that representing such a deviation in the temperature structure increases the surface warming, because the resulting temperature lapse rate (LR) is more similar to a constant LR, showing less temperature increases higher than a moist-adiabatic LR. This effect is likely amplified in a warmer climate due to this mixing process becoming more efficient in pushing the temperature further away from moist-adiabats.

1. Introduction

A moist-adiabatic process describes when a moist air parcel ascends, it cools as it expands and condenses due to saturation. The whole process occurs adiabatically without exchanging heat with the environment. By releasing the fusion enthalpy, condensation acts to partially compensate the cooling due to expansion. The temperature lapse rate (LR) of an air parcel that undergoes this undiluted ascent process is a moist-adiabatic LR. The temperature in the tropical-free troposphere is generally believed to follow a moist-adiabatic LR, because gravity waves generated by deep convection rapidly homogenize the horizontal buoyancy anomaly so as to adjust the density temperature in the nonconvecting regions to that in the convecting regions (Bretherton & Smolarkiewicz, 1989; Mapes, 1993; Sobel & Bretherton, 2000). Therefore, the free-tropospheric temperature in the tropics is set by the regions with deep convection. The key element in the moist-adiabatic definition is that the entire process does not exchange heat with the environment, which is rather something too ambitious to achieve in a realistic context. Still, the moist-adiabatic temperature structure in the tropical atmosphere is supported by some observational studies (Betts, 1986; Xu & Emanuel, 1989).

One idea that goes against a moist-adiabatic thermal structure is that the tropical temperature may not be determined by one or a few strongest convective plumes, but it is rather influenced by the mean effect from all convection occurring (Bao & Stevens, 2021; Singh & O'Gorman, 2013). As a result, to stay moist-adiabatic

throughout the entire free troposphere, the mean convection, consisting of numerous convective parcels, has to be moist-adiabatic. This is an unrealistic idea, because the convection that undergoes moist-adiabatic ascent is extremely rare (Romps & Kuang, 2010). Studies using storm-resolving simulations in the idealized configuration of radiative-convective equilibrium (RCE) show that the tropical temperature tends to deviate from moist-adiabats, because the saturated convective air parcels often mix with the unsaturated environmental air, a process which is referred to as entrainment (Seeley & Romps, 2015; Singh & O'Gorman, 2013, 2015). Entrainment reduces the temperature by pushing the convective air parcels away from the original moist-adiabatic trajectories. Similar temperature deviations from moist-adiabats have also been found in Coupled Model Intercomparison Project Phase 5 models (Miyawaki et al., 2020; Zhou & Xie, 2019). These results suggest that the assumption of a moist-adiabatic structure of tropical temperature may be too simplistic.

To what extent does the tropospheric temperature obey the moist-adiabatic LR? The answer is central to understanding some of the fundamental questions of climate change. The vertical structure of atmospheric warming matters for radiation in two ways: it directly controls the thermal emission of an atmospheric layer, and limits the abundance of water vapor through its saturation value which varies with temperature. These are particularly important for the radiative response to warming, which is often quantified by the LR and water vapor feedbacks. For a moist-adiabatic thermal structure, the enhanced tropospheric warming aloft relative to the surface allows more longwave emission to space than would be the case for a constant LR, enabling a cooler surface temperature—a negative feedback. However, this negative LR feedback is largely counteracted by the corresponding increase of water vapor following roughly the Clausius-Clapeyron relation (Soden & Held, 2006). More water vapor reduces emissivity, leading to warmer surface temperatures: a positive feedback. Changes in this subtle balance between the negative LR feedback and positive water vapor feedback can strongly affect the net feedback, leading to contrasting changes in the equilibrium climate sensitivity (ECS), which is defined as the steady-state temperature increase due to a doubling of the atmospheric CO_2 concentration. It has been shown that the same fractional increase of water vapor at different height alters the net feedback, leading to large changes in ECS (Bourdin et al., 2021; Soden & Held, 2006). Thus, a small departure from the moist-adiabatic structure can potentially have a large impact on the ECS as well.

In this study, we look at the vertical temperature structure and seek to better understand the deviations from moist-adiabats. For simplicity, the moist-adiabatic calculation in this study adopts the pseudo-adiabatic formula as used in Bao and Stevens (2021). We show that these deviations can be explained by different degrees of entrainment, an uncertain parameter controlling the behavior of convective parameterizations in models. Hence, our study allows us to quantify how the specification of entrainment in models may affect their climate sensitivity. The climate sensitivity that we focus on is the clear-sky part of ECS, which we refer to as the clear-sky climate sensitivity ($\mathcal{S}$). We first look into the tropical LR by analyzing the data from a global storm-resolving model. Then a simple hypothesis is proposed to explain the variations in the LR by the entrainment of dry environmental air. Based on this hypothesis, we represent the new temperature profile by taking into account the temperature deviations from moist-adiabats in a one-dimensional clear-sky RCE model—konrad. Finally, we use this model to quantify the impact of temperature deviations from moist-adiabats (and thereby entrainment) on $\mathcal{S}$.

2. Modeling Convection

2.1. Tropical Temperature Deviates From a Moist-Adiabat due to the Impact of Entrainment

We start by investigating the tropical temperature structure from a global storm-resolving model—ICOsahedral Non-hydrostatic model (ICON; Hohenegger et al., 2020; Zängl et al., 2015). The model is configured to run at a quasi-uniform horizontal mesh of 2.5 km for 40 days from August 1 in 2016. The data from the last 10 days of the simulations are used in the analysis. The initial conditions are from the global meteorological analysis at a grid spacing of 9.5 km from the European Center for Medium Range Weather Forecasts and the lower boundary conditions are daily observed sea surface temperatures. Details about the model setup are provided by Hohenegger et al. (2020). Here, we focus on the tropical ocean regions over 10°N–10°S.

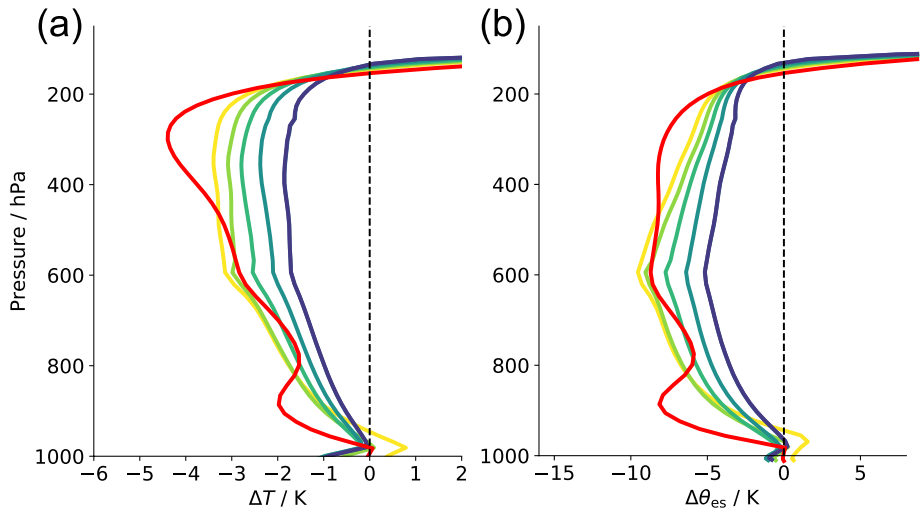

Figure 1. Differences in temperature (ΔT; a) and saturation equivalent potential temperature ($\Delta\theta_{es}$; b) simulated by ICOsahedral Non-hydrostatic model relative to their corresponding moist-adiabatic profiles. The calculations were performed with the model output from the tropical oceans over 10°N–10°S. The moist-adiabatic profiles were calculated based on the domain-mean output from the lowest model level near the surface. Differences are shown for the tropic mean state (red) and the moist regions (colors from yellow to blue correspond to the 90th, 99th, 99.9th, 99.99th, and 99.999th percentile of precipitable water).

Figure 1a shows that the tropical temperature profile is substantially colder than the theoretical moist-adiabat, and this deviation is larger in dry regions where the impact of entrainment is increased. A similar picture is also seen with saturation equivalent potential temperature (θ_{es}). The largest deviation of θ_{es} occurs in the mid-troposphere (600 hPa). Above that the deviation reduces with height. As θ_{es} is a constant for the moist-adiabatic conditions, Figure 1b shows that θ_{es} increases with height above 600 hPa in the ICON simulations.

Such deviation from the moist-adiabat has been attributed to entrainment in convective clouds of environmental air that is usually drier than the parcel itself. This tends to reduce the temperature and pushes the air parcel away from saturation. However, this entrainment effect can only explain the temperature reduction in the lower troposphere. It fails to explain why θ_{es} in relatively drier conditions increases above 600 hPa as shown in Figure 1b. In fact, the increase in θ_{es} with decreasing pressure implies that the temperature in the free troposphere is not regulated by the warmest convection with the highest θ_{es}. If that were the case, the temperature structure throughout the troposphere would suppress convection arising from regions with lower boundary-layer equivalent potential temperature, and the profile of θ_{es} would be more approximately constant throughout the troposphere. However, this is not case as seen in Figure 1b.

We hypothesize that the mean tropical thermal structure reflects the composition of convection happening at different values of boundary-layer equivalent potential temperature (θ_e) and mixing more or less with the environment while rising up, as the temperature in the free troposphere is not determined by the one or a few strongest (or warmest) convection, but rather by the mean convection, which represents a combined effect from all convection occurring over each height. This can be understood with Figure 2. The tropical atmosphere is composed of numerous convective systems. While most convection can reach a relatively lower altitude, the chance of convection occurring at a higher altitude is smaller, and even less can survive up to the tropopause. In order for an air parcel to reach a relatively higher altitude, this parcel has to maintain its positive buoyancy relative to the surrounding environment. Entraining the environmental air into the updraft would successively prevent the parcel from rising higher. As the height that each convective parcel can reach depends on the parcel buoyancy, the upper troposphere is increasingly dominated by the convective parcels that are warmer and more buoyant. These parcels usually arise in a relatively more humid environment so that they can maintain the positive buoyancy. We refer to this height-dependence of parcel buoyancy as the buoyancy sorting of convection. Thus, above a certain level where most air parcels cease to rise, θ_{es} increases with height as shown in Figure 1b, because only the more buoyant air parcels with larger θ_{es} can continue

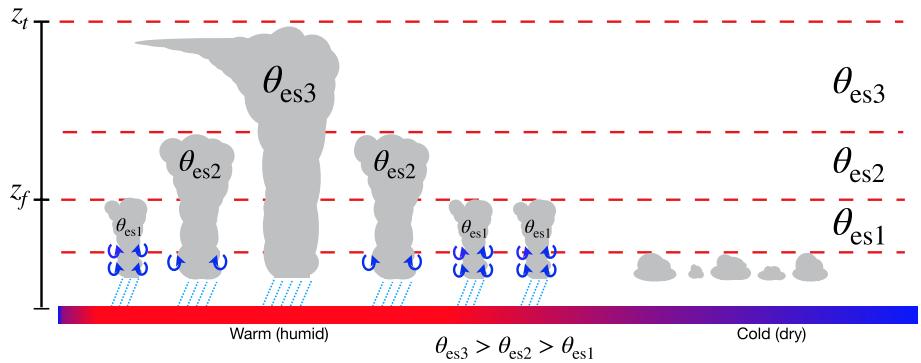

Figure 2. A schematic of tropical convection and temperature. Colors at the surface represent the sea surface temperature. Blue arrows represent the entrainment process. The height of the convective top is denoted by z_t. The freezing level is denoted by z_f.

rising up. This level appears to coincide with the freezing level, which is a stable layer as observed in Johnson et al. (1999) and tends to inhibit cloud growth and promote cloud detrainment (Stevens et al., 2017).

The buoyancy-sorting mechanism has been around for decades and some pioneering studies tried to represent it in convective parameterizations (Emanuel & Živković Rothman, 1999; Raymond & Blyth, 1986). However, it is rarely used to explain the tropical LR changes. One study by Folkins (2002) noticed that the tropical temperature deviates from a moist-adiabat and explained it with the buoyancy-sorting idea. But his results were limited to the tropical tropopause region. Here, we show that the representation of entrainment can affect the temperature profile through the depth of the troposphere. Recently, Zhou and Xie (2019) proposed that the tropical mean temperature structure could not be represented by one convective plume, but rather by a spectral of plumes with different entrainment rates. They developed a spectral plume model with the buoyancy-sorting mechanism to represent the tropical temperature profile.

2.2. Representing the Temperature Deviations From Entrainment in Konrad

We aim to represent the temperature profile that takes into account the deviation from the moist-adiabat in a clear-sky one-dimensional RCE model—konrad (Dacie et al., 2019; Kluft et al., 2019). In konrad, the original convective adjustment assumes that the temperature follows exactly a moist-adiabatic LR, based on the surface temperature calculated by a slab-ocean model. To represent the temperature reduction from the impact of entrainment, we adopt the formula derived from the zero-buoyancy entraining plume model by Singh and O'Gorman (2013). The simulated temperature profiles are compared with the tropical mean profile averaged over the period of 2006–2015 from the ERA5 reanalysis data (Hersbach et al., 2019).

Here, we briefly review the main idea of the zero-buoyancy entraining plume model. The zero-buoyancy entraining plume assumes the cloud buoyancy is small. As the plume is saturated at the environment temperature above the cloud base, this allows us to derive the temperature reduction due to entrainment from the plume moist static energy (MSE) budget:

$$\frac{\mathrm{d}h_{\mathrm{e}}^{*}}{\mathrm{d}z} = -\epsilon\,(h_{\mathrm{e}}^{*} - h_{\mathrm{e}}) = -\epsilon\,\ell_{\mathrm{v}}(q_{\mathrm{ve}}^{*} - q_{\mathrm{ve}}), \tag{1}$$

where ϵ is the entrainment rate, h_{e}^{*} is the saturated MSE at the environment temperature, h_{e} is the MSE of the environment, ℓ_{v} is the latent heat of evaporation, q_{ve}^{*} is the saturation-specific humidity at the environment temperature, and q_{ve} is the specific humidity of the environment.

The MSE of an undiluted parcel (h_{u}) is conserved ($\frac{\mathrm{d}h_{\mathrm{u}}}{\mathrm{d}z} = 0$). This makes the saturation MSE (h_{u}^{*}) above the cloud base also conserved such that $\frac{\mathrm{d}h_{\mathrm{u}}^{*}}{\mathrm{d}z} = 0$. By subtracting Equation 1, we get

$$\frac{\mathrm{d}(h_{\mathrm{u}}^{*} - h_{\mathrm{e}}^{*})}{\mathrm{d}z} = \epsilon\,\ell_{\mathrm{v}}(q_{\mathrm{ve}}^{*} - q_{\mathrm{ve}}). \tag{2}$$

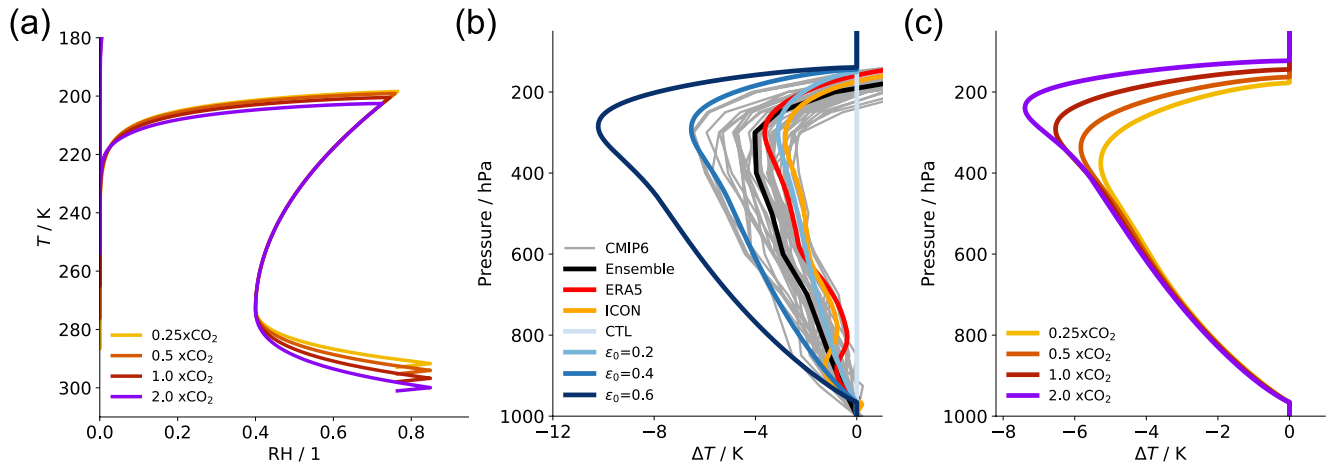

Figure 3. (a) Profiles of relative humidity (RH) in temperature coordinates from the control (CTL) simulations with different CO_2 concentrations. (b) Profiles of temperature deviations (ΔT) from moist-adiabats from konrad simulations of $1\times CO_2$ with different entrainment parameter (ϵ_0), ERA5, ICOsahedral Non-hydrostatic model (ICON), and Coupled Model Intercomparison Project Phase 6 (CMIP6) (black line: multi-model ensemble and gray lines: individual models). (c) Profiles of temperature deviations (ΔT) from moist-adiabats from konrad simulations with different CO_2 concentrations and $\epsilon_0 = 0.4$.

Then we expand h_u^* and h_e^*, and linearize q_v^*:

$$h_u^* - h_e^* = c_p(T_u - T_e) + \ell_v(q_{vu}^* - q_{ve}^*) = \Delta T\left(c_p + \ell_v \frac{\partial q_v^*}{\partial T}\right) \tag{3}$$

where T_u and T_e are the temperature of the undiluted air parcel and the environment, respectively, q_{vu}^* is the saturation-specific humidity at the temperature of the air parcel, ΔT is the temperature difference between the undiluted air parcel and the environment, and c_p is the isobaric specific heat capacity of the dry air. By combining Equations 2 and 3, we integrate vertically to get the temperature reduction from the impact of entrainment (ΔT):

$$\Delta T(z) = \frac{1}{c_p + \ell_v \frac{\partial q_v^*}{\partial T}} \int_{z_b}^{z} \epsilon \ell_v (1 - \mathrm{RH}) q_{ve}^* \mathrm{d}z', \tag{4}$$

where RH is the environmental relative humidity: $\mathrm{RH} \simeq q_{ve}/q_{ve}^*$, and z_b is the height of the cloud base. Equation 4 shows that the temperature reduction from the impact of entrainment depends on the entrainment rate as well as the saturation deficit. Following Romps (2014), RH is predicted by temperature, which exhibits a C shape and is roughly temperature invariant in the free troposphere (Figure 3a). The results are qualitatively consistent if a constant RH profile is used. We use a fixed entrainment rate profile defined as $\epsilon(z) = \epsilon_0/z$ and ϵ_0 is the entrainment parameter. Because konrad uses pressure as its vertical coordinate, the variables simulated by konrad are converted from pressure to height assuming hydrostatic balance before they are used in Equation 4.

The temperature deviation term is not computed strictly from the entraining plume model. For simplicity, we utilize the formula (Equation 4) derived from the model and calculate the temperature deviation term directly. The final temperature profile is obtained by subtracting this temperature deviation term from the temperature assuming the moist-adiabatic adjustment. So we first calculate the moist-adiabatic temperature profile based on the surface temperature, and then use this temperature profile to compute q_{ve}^* in Equation 4. Although q_{ve}^* corresponds to the saturation-specific humidity of the environment, such a simplification would not qualitatively alter the results. Most importantly, the key impact of climate change, that is, the Clausius-Clapeyron increase of q_{ve}^*, is captured.

One major issue with the zero-buoyancy entraining plume model is that it assumes that the temperature in the free troposphere is controlled by the mean convection, but fails to represent the buoyancy sorting of convection. As a result, the upper-tropospheric temperature depicted by the model is unrealistic. Here, to

account for the reduced entrainment effect with height, $\Delta T(z)$ in Equation 4 is weighted by a coefficient $\xi(z)$ defined as:

$$\xi(z) = \begin{cases} \left(\frac{z - z_t}{z_b - z_t}\right)^{\frac{2}{3}}, & z_b \le z \le z_t \\ 0, & \text{elsewhere} \end{cases} \quad (5)$$

where z_t is the height at the convective top, which is determined as the highest level to which convective adjustment is applied, and z_b is the cloud base height which, for simplicity, is kept at the height corresponding to a constant pressure of 960 hPa. Before subtracting from the moist-adiabatic temperature profile, $\Delta T(z)$ is multiplied by $\xi(z)$. $\xi(z)$ varies from 1 at the cloud base to 0 at the convective top, mimicking the reduced entrainment effect with increasing height. The exponent value is tuned so that the temperature deviations are more realistic and Figure 3b shows that our implementation by weighting Equation 4 with Equation 5 reproduces similarly the characteristics of temperature deviations as those in ERA5.

We use konrad to quantify the impact of entrainment-induced deviations from moist-adiabat on the equilibrium surface temperature. Radiation is calculated using the RRTMG radiation scheme (Mlawer et al., 1997). The trace gas concentrations are consistent with those specified in the Radiative-Convective Equilibrium Model Intercomparison Project (Wing et al., 2018). The default CO_2 concentration is 348 ppmv. First, we run a simulation with the moist-adiabatic adjustment at a fixed sea surface temperature (SST) of 298 K. The output from this simulation at the equilibrium state is used to initialize a set of experiments that is forced with a range of CO_2 concentrations from 0.25 to 2 times the default CO_2 concentration. In these simulations, the heat sink of the slab-ocean model is set to be the top-of-atmosphere (TOA) net radiative flux of the fixed SST experiment. For each CO_2 concentration, simulations are performed with two different convective adjustment options: the moist-adiabatic adjustment and the entrainment adjustment. The entrainment effect is investigated by varying the entrainment parameter ϵ_0 from 0.2 to 0.6. The simulations with the moist-adiabatic adjustment are the control (CTL) experiments and can be viewed as $\epsilon_0 = 0$. Additionally, to assist in interpretation, we run simulations with a fixed LR of 6.5 K km^{-1}.

When estimating forcings and feedbacks, we want to compare simulations that only differ in their CO_2 concentrations. Therefore, each perturbed simulation is initialized with data from a simulation that uses the same configuration but the default CO_2 concentration. In this study, $\mathcal{S}$ is calculated as the SST change from those simulations of a doubling of CO_2 relative to the initial SST. The forcing ($\Delta F_{2\times CO_2}$) is the radiative imbalance per CO_2 doubling. Then, the climate feedback parameter is defined as:

$$\lambda = -\frac{\Delta F_{2\times CO_2}}{\mathcal{S}}. \quad (6)$$

Following the method introduced by Gregory et al. (2004), we regress changes in the TOA radiative flux against changes in SST for the daily mean output (Figure S1). The data over the initial period of stratospheric adjustment are excluded. As konrad is an idealized model in which many processes are either neglected or simplified, the uncertainty in the regression analysis is extremely small. We obtain almost perfect linear relationships between TOA radiative imbalance and SST change. The intercept of the regression line gives the effective radiative forcing ($\Delta F_{2\times CO_2}$), and the regression slope is the feedback parameter (λ).

3. LR Effects on Climate Sensitivity

Figure 3b shows the profiles of temperature deviations from the moist-adiabats simulated by konrad. Due to the impact of entrainment, the free troposphere is colder. This cooling effect is increased with a larger entrainment parameter (ϵ_0). The profile simulated by konrad with $\epsilon_0 = 0.2$ best fits the ERA5 profile. Thus, by including a weighted temperature deviation term derived from the zero-buoyancy entraining plume model, our implementation in konrad well captures the main characteristics of the tropical temperature structure.

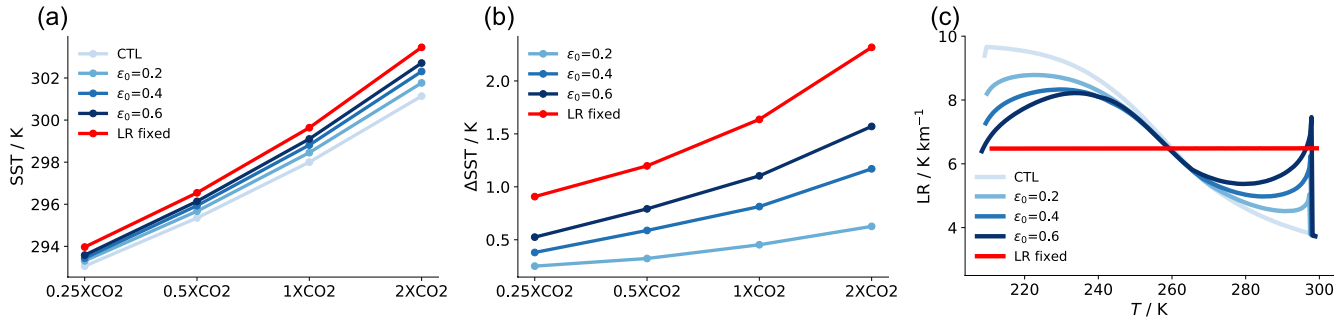

Figure 4. (a) Sea surface temperature (SST) at the equilibrium states as a function of CO_2 concentration. (b) SST changes as a function of CO_2 concentration. SST changes are computed using SSTs from different experiments as shown in (a) minus the SSTs from control (CTL). (c) Lapse rate (LR) as a function of atmospheric temperature (T) from the simulations of $1 \times CO_2$.

Figure 4a shows SST in equilibrium from the konrad simulations. In the CTL simulations, which use a moist-adiabatic adjustment, SST is the lowest, increasing from 293.1 K in $0.25 \times CO_2$ to 301.1 K in $2 \times CO_2$. The highest SSTs occur in simulations with a fixed LR, ranging from 294 K in $0.25 \times CO_2$ to 303.5 K in $2 \times CO_2$. With the impact of entrainment, SST values change between those from the CTL simulations and those from simulations with a fixed LR. With the same CO_2 concentration, a stronger entrainment effect (larger ϵ_0) tends to increase SST. Increasing CO_2 concentration further amplifies the surface warming due to entrainment. This is because according to Equation 4, the impact of entrainment in reducing the temperature is more pronounced in a warmer climate due to the upward shift in the height of convection and also the increase in the saturation deficit that is controlled by the Clausius-Clapeyron relation (Figure 3c). Thus, our model predicts that even with the same entrainment rate, the temperature deviations from entrainment can lead to more amplified surface warming as CO_2 concentration increases. This extra warming effect will add up to the expected warming from rising CO_2 concentration, promoting an even warmer climate.

With a larger entrainment effect, $\mathcal{S}$ increases consistently from 3.1 K in CTL to 3.6 K in the simulation of $\epsilon_0 = 0.6$ (Table 1). This is mainly because of the weakening in λ. In general, cooling in the free troposphere would weaken the negative LR feedback, which is expected to be balanced by a corresponding decrease in the positive water vapor feedback. However, as the magnitude of the total feedback decreases with stronger entrainment effect, it suggests that the positive water vapor feedback does not weaken as much to balance the reduction in negative LR feedback. This is consistent with Bourdin et al. (2021) who used the same model and found that the changes in the LR feedback dominate at low absolute humidities for a vertically uniform profile of RH < 0.75 at roughly present-day temperature. Due to changes in the effective emission height, perturbing the humidity at different heights in the troposphere can lead to contrasting responses in $\mathcal{S}$: increasing the water vapor in the upper troposphere enhances $\mathcal{S}$, while increasing the water vapor in the lower mid-troposphere reduces $\mathcal{S}$ (Bourdin et al., 2021). As a result, the total feedback change and $\mathcal{S}$ are controlled by the LR feedback change. Indeed, entrainment cooling causes drying in both the upper and lower troposphere. While drying in the upper troposphere tends to reduce $\mathcal{S}$, this is compensated, at least partially, by the drying in the lower troposphere, which increases $\mathcal{S}$. Therefore, the total water vapor feedback change is moderated. Meanwhile, we find that a larger entrainment effect alters the LR in a way that more closely resembles a constant LR (Figure 4c). Therefore, the negative LR feedback is weakened and $\mathcal{S}$ is enhanced.

Table 1
Summary of the Clear-Sky Climate Sensitivity ($\mathcal{S}$), Forcing ($\Delta F_{2\times CO_2}$), and Feedback (λ)

Experiments	$\mathcal{S}$/K	$\Delta F_{2\times CO_2}$/Wm^{-2}	λ / Wm^{-2}K^{-1}
CTL	3.14	4.89	−1.56
$\epsilon_0 = 0.2$	3.31	4.92	−1.49
$\epsilon_0 = 0.4$	3.49	4.94	−1.41
$\epsilon_0 = 0.6$	3.59	4.94	−1.38
LR fixed	3.82	5.08	−1.33

Note. CTL, control; LR, lapse rate.

Finally, we compare the results from the Atmospheric Model Intercomparison Project experiments by the models taking part in Coupled Model Intercomparison Project Phase 6 (CMIP6; Eyring et al., 2016). We select the data over the period of 2006–2015 and calculate the tropical mean temperature deviations from moist-adiabats. In general, CMIP6 models are able to represent the overall temperature deviations from moist-adiabats, albeit with substantial spread in the free troposphere by individual models (Figure 3b). The temperature deviations in CMIP6 are roughly equivalent to those sim-

ulated in konrad with ϵ_0 between less than 0.2 and 0.4. This would lead to 0.2 K ~ 0.3 K spread in $\mathcal{S}$. The spread in $\mathcal{S}$ in our simulations is mainly driven by a decrease in λ. Note that this change in clear-sky λ could cause a larger spread in all-sky ECS due to the nonlinear dependence of climate sensitivity on the feedback parameter. Hence, the simulated biases would be expected to contribute to the uncertainties in model estimation of ECS.

4. Conclusions

We show that the tropical temperature in the free troposphere deviates substantially from a theoretical moist-adiabat in a global storm-resolving model. The overall deviations are attributed to the impact of entrainment—the mixing of saturated convective air parcels with unsaturated environmental air. The temperature deviations approach zero in the upper troposphere, which we explain with a buoyancy-sorting mechanism: the height to which individual convective parcels rise depends on its buoyancy, which is closely tied to how much environmental air it entrains during ascent. While the lower troposphere, which is easier to reach, is dominated by most of the convection, the upper troposphere is increasingly controlled by the convection that is warmer and more buoyant, and is less affected by entrainment.

We represent such temperature deviations from moist-adiabats in a clear-sky one-dimensional RCE model and quantify its impact on the clear-sky climate sensitivity ($\mathcal{S}$). The temperature deviation term is represented by weighting the formula derived from a zero-buoyancy entraining plume model with a height-dependent coefficient. We show that this idealized representation of entrainment is capable of producing temperature profiles more similar to the ERA5 reanalysis. Compared with a strict moist-adiabatic adjustment, having this entrainment-induced temperature deviation leads to higher $\mathcal{S}$, because entrainment alters the LR in a way that more closely resembles a constant LR. This weakens the negative LR feedback. Meanwhile, the positive water vapor feedback changes less due to compensating effects from drying in the upper and lower troposphere. Thus, $\mathcal{S}$ increases because the total feedback change is dominated by the change in the LR feedback. Finally, as the impact of entrainment depends on the saturation deficit, which increases with warming due to the Clausius-Clapeyron relation, this model predicts even more amplified surface warming from entrainment in a warmer climate.

Although uncertainties in projected warming are largely contributed by the cloud feedback, this study emphasizes the importance of understanding how the clear-sky feedbacks change with warming. The CMIP6 model ensemble is capable of replicating the observed temperature deviations from moist-adiabats. Still, the spread in temperature deviations among individual models can contribute to the $\mathcal{S}$ uncertainty of 0.2 K ~ 0.3 K.

Entrainment and its impact on LR can potentially influence clouds and circulation, which are not represented by our simple model. Results from idealized RCE simulations show that increased impact of entrainment can lead to more organized convection (Tompkins & Semie, 2017), and climate sensitivity is associated with changes in the degree of organization (Becker & Wing, 2020). A recent observational study showed that deep convective organization modulates tropical radiation budget, which is expected to affect climate sensitivity (Bony et al., 2020). Thus, an improved understanding of the impact of entrainment on climate sensitivity through clouds and circulation is desired.

Data Availability Statement

The konrad model source code is available on https://doi.org/10.5281/zenodo.1313687. ERA5 data (Hersbach et al., 2019) were downloaded from the Copernicus Climate Change Service (C3S) Climate Data Store (https://cds.climate.copernicus.eu/cdsapp#!/dataset/reanalysis-era5-pressure-levels-monthly-means?tab=overview). The CMIP6 data are made available for this study by the DKRZ and can be obtained from the ESGF at https://esgf-data.dkrz.de/projects/cmip6-dkrz/. The KONRAD run scripts and code for reproducing the plots are available on MPG publication repository (http://hdl.handle.net/21.11116/0000-0008-FDA6-0).

Acknowledgments
The authors thank Steven Sherwood, Julia Windmiller, Tobias Becker, and Cathy Hohenegger for discussion and comments. The authors thank Hans Mikhail Segura Cajachagua for the internal review of the manuscript. The authors thank two anonymous reviewers for insightful feedback. ICON output from the DYAMOND project was provided by the German Climate Computing Center (DKRZ) and supported through the projects ESiWACE and ESiWACE2. Open access funding enabled and organized by Projekt DEAL.

References

Bao, J., & Stevens, B. (2021). The elements of the thermodynamic structure of the tropical atmosphere. *Journal of the Meteorological Society of Japan. Ser. II*. https://doi.org/10.2151/jmsj.2021-072

Becker, T., & Wing, A. A. (2020). Understanding the extreme spread in climate sensitivity within the radiative-convective equilibrium model intercomparison project. *Journal of Advances in Modeling Earth Systems*, *12*(10), e2020MS002165. https://doi.org/10.1029/2020MS002165

Betts, A. K. (1986). A new convective adjustment scheme. Part I: Observational and theoretical basis. *Quarterly Journal of the Royal Meteorological Society*, *112*(473), 677–691. https://doi.org/10.1002/qj.49711247307

Bony, S., Semie, A., Kramer, R. J., Soden, B., Tompkins, A. M., & Emanuel, K. A. (2020). Observed modulation of the tropical radiation budget by deep convective organization and lower-tropospheric stability. *AGU Advances*, *1*(3), e2019AV000155. https://doi.org/10.1029/2019AV000155

Bourdin, S., Kluft, L., & Stevens, B. (2021). Dependence of climate sensitivity on the given distribution of relative humidity. *Geophysical Research Letters*, *48*(8), e2021GL092462. https://doi.org/10.1029/2021GL092462

Bretherton, C. S., & Smolarkiewicz, P. K. (1989). Gravity waves, compensating subsidence and detrainment around cumulus clouds. *Journal of the Atmospheric Sciences*, *46*(6), 740–759. https://doi.org/10.1175/1520-0469(1989)046<0740:GWCSAD>2.0.CO;2

Dacie, S., Kluft, L., Schmidt, H., Stevens, B., Buehler, S. A., Nowack, P. J., et al. (2019). A 1D RCE study of factors affecting the tropical tropopause layer and surface climate. *Journal of Climate*, *32*(20), 6769–6782. https://doi.org/10.1175/JCLI-D-18-0778.1

Emanuel, K. A., & Živković Rothman, M. (1999). Development and evaluation of a convection scheme for use in climate models. *Journal of the Atmospheric Sciences*, *56*(11), 1766–1782. https://doi.org/10.1175/1520-0469(1999)056<1766:DAEOAC>2.0.CO;2

Eyring, V., Bony, S., Meehl, G. A., Senior, C. A., Stevens, B., Stouffer, R. J., & Taylor, K. E. (2016). Overview of the Coupled Model Intercomparison Project Phase 6 (CMIP6) experimental design and organization. *Geoscientific Model Development*, *9*(5), 1937–1958. https://doi.org/10.5194/gmd-9-1937-2016

Folkins, I. (2002). Origin of lapse rate changes in the upper tropical troposphere. *Journal of the Atmospheric Sciences*, *59*(5), 992–1005. https://doi.org/10.1175/1520-0469(2002)059<0992:oolrci>2.0.co;2

Gregory, J. M., Ingram, W. J., Palmer, M. A., Jones, G. S., Stott, P. A., Thorpe, R. B., et al. (2004). A new method for diagnosing radiative forcing and climate sensitivity. *Geophysical Research Letters*, *31*(3). https://doi.org/10.1029/2003GL018747

Hersbach, H., Bell, B., Berrisford, P., Biavati, G., Horányi, A., Muñoz Sabater, J., et al. (2019). *ERA5 monthly averaged data on pressure levels from 1979 to present*. Copernicus Climate Change Service (C3S) Climate Data Store (CDS). https://doi.org/10.24381/cds.6860a573

Hohenegger, C., Kornblueh, L., Klocke, D., Becker, T., Cioni, G., Engels, J. F., et al. (2020). Climate statistics in global simulations of the atmosphere, from 80 to 2.5 km grid spacing. *Journal of the Meteorological Society of Japan Series II*, *98*(1), 2020–005–91. https://doi.org/10.2151/jmsj.2020-005

Johnson, R. H., Rickenbach, T. M., Rutledge, S. A., Ciesielski, P. E., & Schubert, W. H. (1999). Trimodal characteristics of tropical convection. *Journal of Climate*, *12*(8), 2397–2418. https://doi.org/10.1175/1520-0442(1999)012<2397:tcotc>2.0.co;2

Kluft, L., Dacie, S., Buehler, S. A., Schmidt, H., & Stevens, B. (2019). Re-examining the first climate models: Climate sensitivity of a modern radiative–convective equilibrium model. *Journal of Climate*, *32*(23), 8111–8125. https://doi.org/10.1175/JCLI-D-18-0774.1

Mapes, B. E. (1993). Gregarious tropical convection. *Journal of the Atmospheric Sciences*, *50*(13), 2026–2037. https://doi.org/10.1175/1520-0469(1993)050<2026:gtc>2.0.co;2

Miyawaki, O., Tan, Z., Shaw, T. A., & Jansen, M. F. (2020). Quantifying key mechanisms that contribute to the deviation of the tropical warming profile from a moist adiabat. *Geophysical Research Letters*, *47*(20), e2020GL089136. https://doi.org/10.1029/2020GL089136

Mlawer, E. J., Taubman, S. J., Brown, P. D., Iacono, M. J., & Clough, S. A. (1997). Radiative transfer for inhomogeneous atmospheres: RRTM, a validated correlated-k model for the longwave. *Journal of Geophysical Research*, *102*(D14), 16663–16682. https://doi.org/10.1029/97JD00237

Raymond, D. J., & Blyth, A. M. (1986). A stochastic mixing model for nonprecipitating cumulus clouds. *Journal of the Atmospheric Sciences*, *43*(22), 2708–2718. https://doi.org/10.1175/1520-0469(1986)043<2708:asmmfn>2.0.co;2

Romps, D. M. (2014). An analytical model for tropical relative humidity. *Journal of Climate*, *27*(19), 7432–7449. https://doi.org/10.1175/JCLI-D-14-00255.1

Romps, D. M., & Kuang, Z. (2010). Do undiluted convective plumes exist in the upper tropical troposphere? *Journal of the Atmospheric Sciences*, *67*(2), 468–484. https://doi.org/10.1175/2009jas3184.1

Seeley, J. T., & Romps, D. M. (2015). Why does tropical convective available potential energy (cape) increase with warming? *Geophysical Research Letters*, *42*(23), 10429–10437. https://doi.org/10.1002/2015GL066199

Singh, M. S., & O'Gorman, P. A. (2013). Influence of entrainment on the thermal stratification in simulations of radiative-convective equilibrium. *Geophysical Research Letters*, *40*(16), 4398–4403. https://doi.org/10.1002/grl.50796

Singh, M. S., & O'Gorman, P. A. (2015). Increases in moist-convective updraught velocities with warming in radiative-convective equilibrium. *Quarterly Journal of the Royal Meteorological Society*, *141*(692), 2828–2838. https://doi.org/10.1002/qj.2567

Sobel, A. H., & Bretherton, C. S. (2000). Modeling tropical precipitation in a single column. *Journal of Climate*, *13*, 4378–4392. https://doi.org/10.1175/1520-0442(2000)013<4378:mtpias>2.0.co;2

Soden, B. J., & Held, I. M. (2006). An assessment of climate feedbacks in coupled ocean-atmosphere models. *Journal of Climate*, *19*(14), 3354–3360. https://doi.org/10.1175/JCLI3799.1

Stevens, B., Brogniez, H., Kiemle, C., Lacour, J.-L., Crevoisier, C., & Kiliani, J. (2017). Structure and dynamical influence of water vapor in the lower tropical troposphere. *Surveys in Geophysics*, *38*(6), 1371–1397. https://doi.org/10.1007/s10712-017-9420-8

Tompkins, A. M., & Semie, A. G. (2017). Organization of tropical convection in low vertical wind shears: Role of updraft entrainment. *Journal of Advances in Modeling Earth Systems*, *9*(2), 1046–1068. https://doi.org/10.1002/2016MS000802

Wing, A. A., Reed, K. A., Satoh, M., Stevens, B., Bony, S., & Ohno, T. (2018). Radiative–convective equilibrium model intercomparison project. *Geoscientific Model Development*, *11*(2), 793–813. https://doi.org/10.5194/gmd-11-793-2018

Xu, K.-M., & Emanuel, K. A. (1989). Is the tropical atmosphere conditionally unstable? *Monthly Weather Review*, *117*, 1471–1479. https://doi.org/10.1175/1520-0493(1989)117<1471:ittacu>2.0.co;2

Zängl, G., Reinert, D., Rípodas, P., & Baldauf, M. (2015). The ICON (icosahedral non-hydrostatic) modelling framework of DWD and MPI-M: Description of the non-hydrostatic dynamical core. *Quarterly Journal of the Royal Meteorological Society*, *141*(687), 563–579. https://doi.org/10.1002/qj.2378

Zhou, W., & Xie, S.-P. (2019). A conceptual spectral plume model for understanding tropical temperature profile and convective updraft velocities. *Journal of the Atmospheric Sciences*, *76*(9), 2801–2814. https://doi.org/10.1175/JAS-D-18-0330.1